A Co-Fe Prussian blue analogue for efficient Fenton-like catalysis: the effect of high-spin cobalt

Chunxiao Zhao[a,b†], Biao Liu[c†], Xuning Li[d], Kaixin Zhu[b], Ruisheng Hu[a,] Zhimin Ao[c,*], and Junhu Wang[b,*]

[a]*College of Chemistry and Chemical Engineering, Inner Mongolia University, Hohhot 010021, China*

[b]*Mössbauer Effect Data Center, Dalian Institute of Chemical Physics, Chinese Academy of Sciences, Dalian 116023, China*

[c]*Guangzhou Key Laboratory of Environmental Catalysis and Pollution Control, Institute of Environmental Health and Pollution Control, School of Environmental Science and Engineering, Guangdong University of Technology, Guangzhou 510006, China*

[d]*School of Chemical and Biomedical Engineering, Nanyang Technological University, 62 Nanyang Drive, Singapore 637459, Singapore*

[†] *These authors contributed equally to this work.*

Materials and chemicals

Potassium hexacyanoferrate, cobaltous chloride, ferrous chloride, Nickel Nitrate and Cupric nitrate were purchased from Tianjin Daomao Chemical Reagent Co., Ltd., China. Potassium hexacyanocobaltate(III) (98%) was purchased from Beijing J&K Co., Ltd., China. 5,5-dimethyl-1-pyrroline-N-oxide (DMPO) and bisphenol A (BPA) were purchased from Aladdin Co., China. Methanol and t-butanol (TBA) were acquired from Tianjin Kermel Chemical Reagent Co., Ltd., China. Monopersulfate (PMS) was purchased from Alfa Aesar Co., China. All chemical reagents were used without further purification.

Preparation of Co–Fe PBA

$Co_3[Fe(CN)_6]_2{\cdot}10H_2O$ (Co–Fe PBA) was prepared by reaction of aqueous solutions of $CoCl_2{\cdot}6H_2O$ and $K_3[Fe(CN)_6]$. 20 mL $K_3[Co(CN)_6]$ aqueous solution (0.1 M) was slowly added into 20 mL $CoCl_2{\cdot}6H_2O$ aqueous solution (0.15 M) under magnetic stirring. The mixed solution was further stirred for another 30 min and aged for 12 h. Finally, the resulting precipitates were centrifuged and washed for at least three times with deionized water, followed by drying in an oven at 333 K for 12 h. For comparison, the Fe-Co PBA was synthesized by the same process as that of Co–Fe PBA, except the replacement of $K_3[Fe(CN)_6]$ (0.10 M) using $K_3[Co(CN)_6]$ (0.10 M) and the replacement of $CoCl_2{\cdot}6H_2O$ (0.15 M) using $FeCl_2{\cdot}4H_2O$ (0.15 M). The Co-Co PBA was also synthesized by the same process as that of Co–Fe PBA, except the replacement of $K_3[Fe(CN)_6]$ (0.10 M) using $K_3[Co(CN)_6]$ (0.10 M). The Cu–Fe PBA, Ni–Fe PBA and Fe–Fe PBA were also synthesized by the similar process of Co–Fe PBA, but with $Cu(NO_3)_2{\cdot}3H_2O$, Ni $(NO_3)_2{\cdot}6H_2O$ and $FeCl_2{\cdot}4H_2O$ as the metal precursors, respectively.

Characterization of Co–Fe PBA

The X-ray diffraction (XRD) patterns were measured on a PANalytical X'Pert-Pro X-ray

*Corresponding authors. Email: wangjh@dicp.ac.cn, zhimin.ao@gdut.edu.cn.

diffractometer equipped with Ni-filtered Cu Kα (λ = 0.15406 nm) radiation source in an angular range of 2θ from 10° to 80°. The surface morphologies were studied using a Tecnai G2 Spirit transmission electron microscopy (TEM) with an accelerating voltage of 120 kV. The X-ray photoelectron spectra (XPS) were measured on an ESCALAB 250 X-ray photoelectron spectroscope equipped with monochromated Al Kα source. All binding energies were calibrated by a standard sample of carbon (C 1 s = 284.8 eV). The spectra were fitted by the XPSPEAK41 software using Shirley-type background. The room temperature ^{57}Fe Mössbauer spectra were recorded using a proportional counter and a Topologic 500A spectrometer with ^{57}Co (Rh) as a γ-ray radioactive source. The electron spin-resonance spectroscopy (ESR) carried out in the Fenton-like process were obtained using a Brucker ESR I200 spectrometer with the sweep width of 100 G and a center field at 3320 G at room temperature. The detailed procedures of Mössbauer and ESR measurements can be found in our previous work. [1]

Catalytic activity measurements of Co–Fe PBA

The catalytic performance of the Co–Fe PBA was evaluated by activation of PMS (0.1 g L^{-1}) for removal of BPA in water (20 mg L^{-1}) at pH 6.0 in a dark box. The reaction temperature was kept at 308 K. If necessary, the pH value was adjusted by either 0.1 M NaOH or 0.1 M HNO_3 aqueous solution and recorded by an Orion pH meter (model PHSJ-3F).

In all experiments, 5 mg catalyst was added into a 50 mL BPA solution (20 mg L^{-1}) and stirred for 30 min to establish the adsorption–desorption equilibrium. The reaction was initiated by adding certain amounts of PMS. At given reaction time intervals, samples (1 mL) were withdrawn, immediately quenched with 1 mL ethanol and then centrifuged. In each recyclability test, the catalyst was collected by centrifugation and washed thoroughly with deionized water.

The concentration of BPA was analyzed by a high performance liquid chromatography (HPLC, Shimadzu, 2030) with a C18 column. The mobile phases are acetonitrile and water. The injection gradient was: initial conditions of 30% acetonitrile with a 5 min hold, then up to 50% at 13.5 min and held for 1.5 min, then up to 95% at 21 min and held for 9 min. The detection wavelength was set at 230 nm.

The reaction rate was evaluated by a first order kinetics model as the following equation: $\ln(C_0/C_t) = k\ t$, where C_0 and C_t are the initial and the instantaneous concentrations respectively, k is the rate constant, and t is the reaction time.

Computational framework

Density functional theory (DFT) calculations in this work were performed by using Dmol3 package. [2] Exchange correlation function was generalized gradient approximation (GGA) with PBE. Localized double numerical plus polarization (DNP) basis sets were employed to expand the Kohn–Sham orbitals. The convergence tolerance of energy is $1.0e^{-5}$ eV/atom, and the maximum-allowed displacement and force are 0.002 Å and 0.05eV/Å, respectively. The DFT-D method was used for all calculations to consider the van der Waals forces. To avoid the interaction of surfaces in different supercells along c direction, a 20 Å vacuum above the slab surface were taken. All atoms were allowed to relax except the bottom three layers atoms were fixed at the ground-state bulk positions. Charge transfers were calculated with the Milliken charge analysis method. To investigate the minimum energy pathway (MEP) for free radical production from PMS molecules, linear synchronous transition/quadratic synchronous transit (LST/QST) and nudged

elastic band (NEB) tools in Dmol3 code were used, [3,4] which have been well validated to find the transition state (TS) structure and the MEP. [4,5]

For one peroxymonosulfate (PMS) molecule adsorbed on Prussian blue analogues (PBAs), the adsorption energy E_{ads} is defined as:

$$E_{ads} = E_{PBAs+PMS} - E_{PBAs} - E_{PMS} \quad (1)$$

where $E_{PBAs+PMS}$, E_{PBAs} and E_{PMS} are energies of PBAs with PMS adsorption, isolate PBAs and free PMS molecule, respectively.

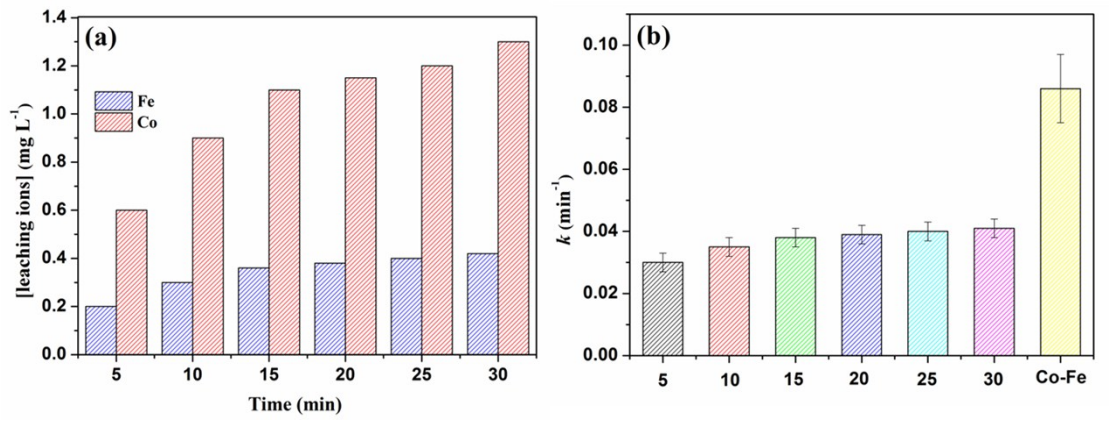

Fig. S1. (a) The concentrations of the leached Fe/Co ions and (b) the rate constants of the leached Fe/Co ions at different reaction times compared with that of Co-Fe PBA. The k of the total reaction catalyzed by Co-Fe PBA (0.086 min^{-1}) was more than two times higher than that of the homogeneous reaction, suggesting the dominant role of the heterogeneous reaction.

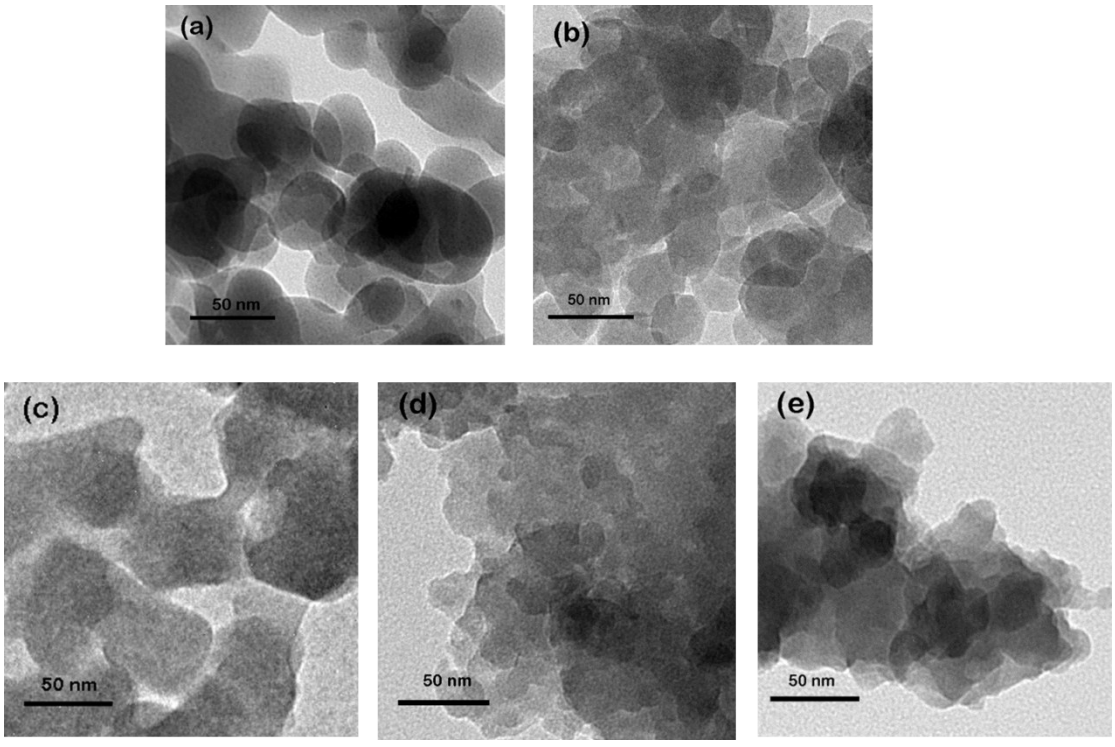

Fig. S2. TEM images of (a) Fe-Co PBA, (b) Co-Fe PBA, (c) Cu-Fe PBA, (d) Ni-Fe PBA, and (e) Fe -Fe PBA.

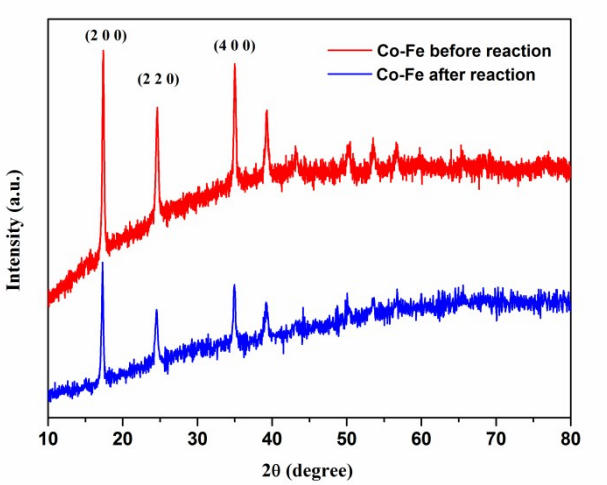

Fig. S3. XRD patterns of Co-Fe PBA before and after reaction.

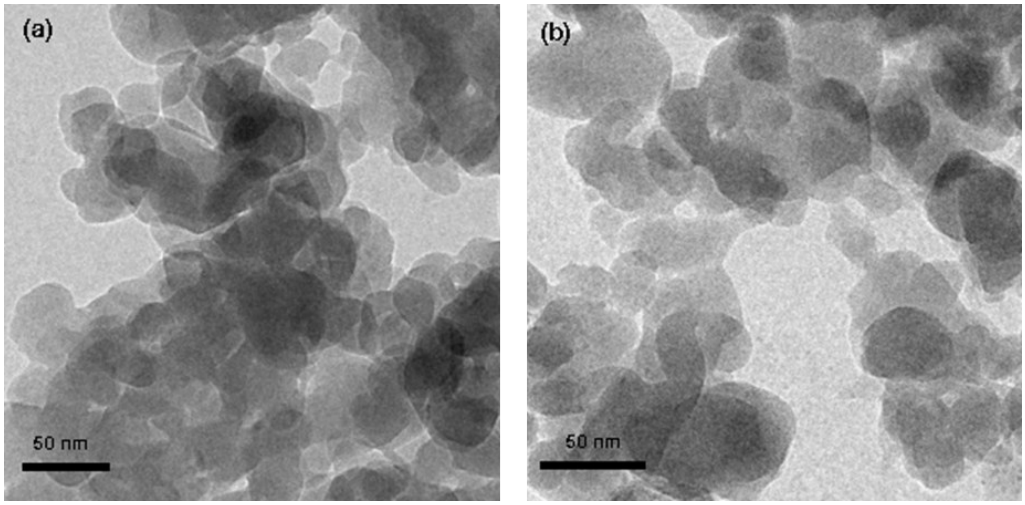

Fig. S4. TEM images of Co-Fe PBA: (a) before and (b) after reaction.

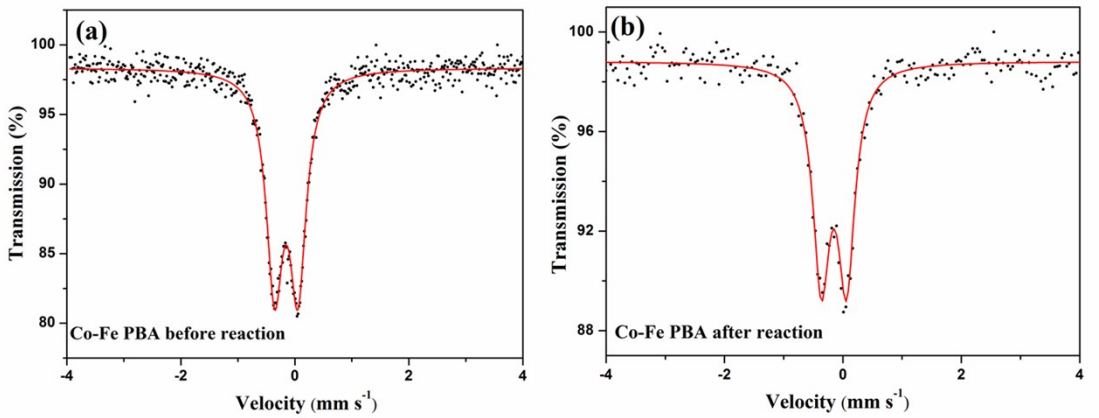

Fig. S5. Mössbauer spectra of Co-Fe PBA before and after reaction.

Table S1 The catalytic performance comparison of recently reported PBAs for PMS/ H_2O_2 activation.

Catalyst (loading, g L^{-1})	PMS[a]/H_2O_2[b] (g L^{-1})/ (mmol L^{-1})	Pollutant (mg L^{-1})	Removal efficiency	Ref.
Co-Fe PBA (0.1)	0.1 a	BPA (20)	93% (30 min)	This work
Cu-Fe PBA (0.1)	0.1 a	BPA (20)	7% (30 min)	This work
Ni-Fe PBA (0.1)	0.1 a	BPA (20)	3% (30 min)	This work
Fe-Fe PBA (0.1)	0.1 a	BPA (20)	12% (30 min)	This work
Co-Co PBA (0.1)	0.1 a	BPA (20)	93% (30 min)	This work
Fe-Co PBA (0.1)	0.1 a	BPA (20)	48% (30 min)	This work
Fe-Co PBA (0.2)	4 b	RhB (12)	93% (30 min)	6
Fe-Co PBA (0.2)	0.05 a	BPA (20)	79% (240 min)	7
Co-Fe PBA/graphene (0.05)	0.6 a	Levofloxacin (20)	97.6% (30 min)	8
Bi-Fe PBA (0.01)	5 b + vis	RhB (10)	96% (10 min)	9

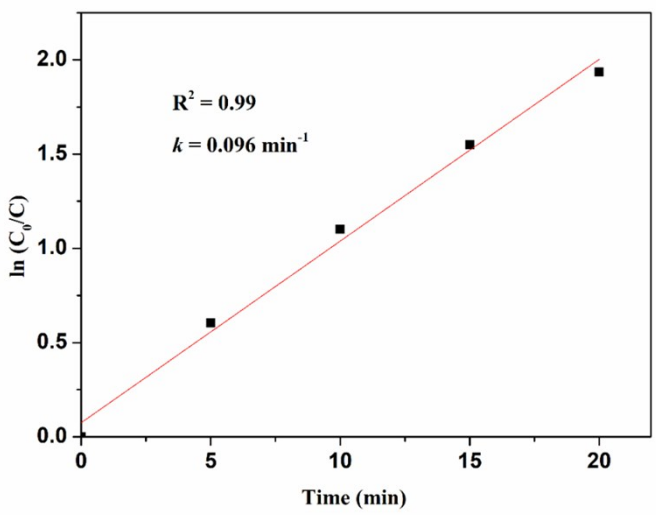

Fig. S6. Kinetic behavior of BPA degradation reaction in the Co-Fe PBA/PMS system. Reaction conditions: [BPA] = 20 mg L^{-1}, [PMS] = 0.1 g L^{-1}, catalyst = 0.1 g L^{-1} , T = 308 K, initial solution pH = 6.0.

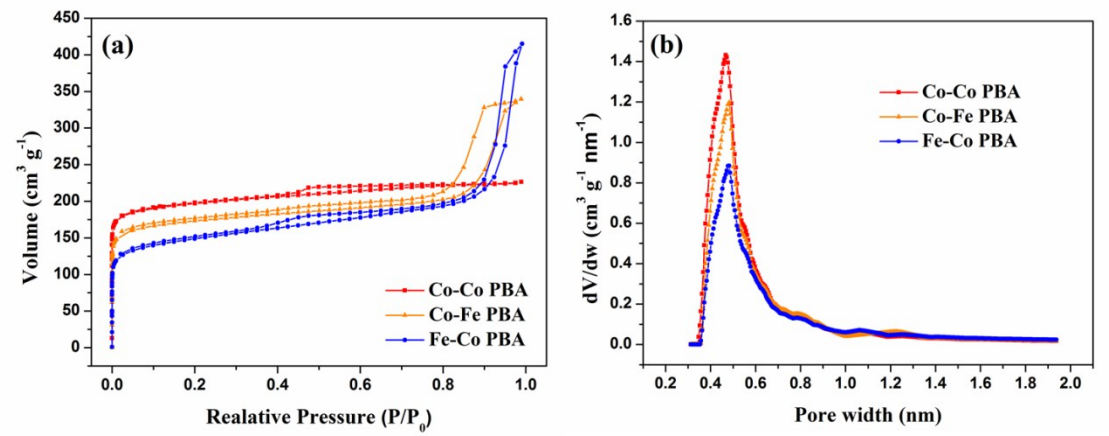

Fig. S7. (a) N2 adsorption/desorption isotherm; (b) the pore size distribution of Co-Fe PBA, Fe-Co PBA and Co-Co PBA.

Table S2. BET surface, pore size and micropore volume of Co-Fe PBA, Fe-Co PBA and Co-Co PBA.

Sample	Co-Co PBA	Co-Fe PBA	Fe-Co PBA
BET (m^2/g)	767.893	669.003	555.591
H-K median Pore width (nm)	0.468	0.483	0.483
micropore Volume (cm^3/g)	0.268	0.224	0.163

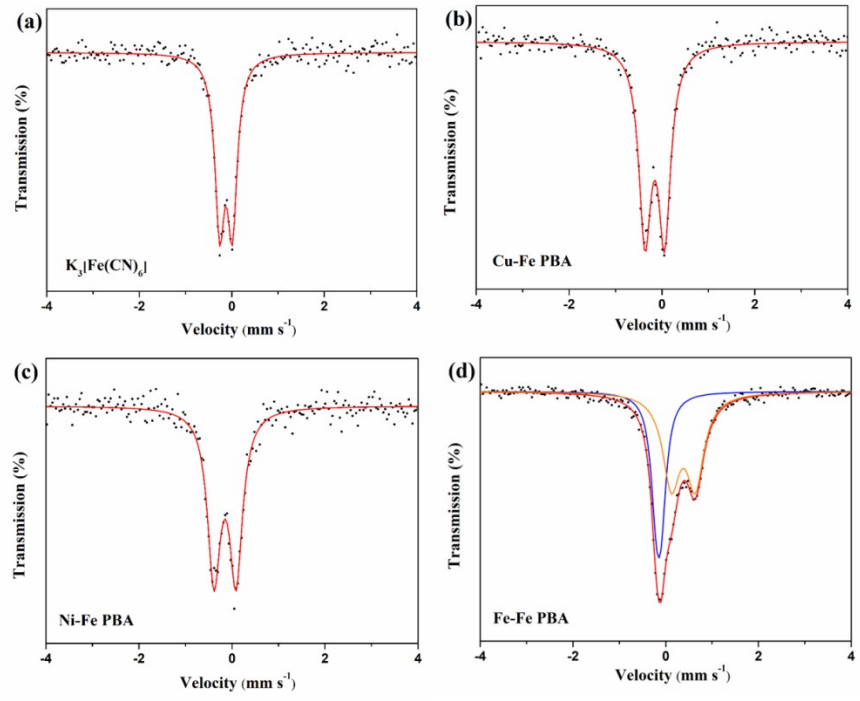

Fig. S8. Room temperature ^{57}Fe Mössbauer spectra of (a) precursor $K_3[Fe(CN)_6]$, and (b)-(d) M-Fe PBAs (M = Cu, Ni, Fe). The spectra of (a)-(c) were all fitted with a quadrupole doublet and all the doublets could be assigned to low-spin Fe^{III}. The spectrum of (d) was fitted with two quadrupole

doublets, which could be separately assigned to low-spin Fe^{II} (blue line) and high-spin Fe^{III} (orange line), as same as that of pristine Prussian blue.

Table S3. Room temperature ^{57}Fe Mössbauer parameters of $K_3[Fe(CN)_6]$, M-Fe PBAs (M = Cu, Ni, Fe), Fe-Co PBA, and Co-Fe PBA before and after Fenton-like reaction.

Sample	Spin state	IS (mm s^{-1})	QS (mm s^{-1})	Line width (mm s^{-1})	Spectral area (%)
$K_3[Fe(CN)_6]$	LS Fe^{III}	-0.12	0.27	0.25	100
Cu-Fe PBA	LS Fe^{III}	-0.15	0.42	0.32	100
Ni-Fe PBA	LS Fe^{III}	-0.15	0.47	0.34	100
Fe-Fe PBA	LS Fe^{II}	-0.15	0.11	0.28	40
	HS Fe^{III}	0.38	0.52	0.46	60
Fe-Co PBA	HS Fe^{III}	0.30	0.48	0.39	18
	HS Fe^{II}	1.15	0.88	0.39	27
		1.13	1.47	0.39	18
		1.14	1.87	0.39	37
Co-Fe PBA	LS Fe^{III}	-0.15	0.41	0.35	100

IS: isomer shift, the IS value is relative to the α-Fe; QS: quadrupole splitting; LS: low spin; HS: high spin.

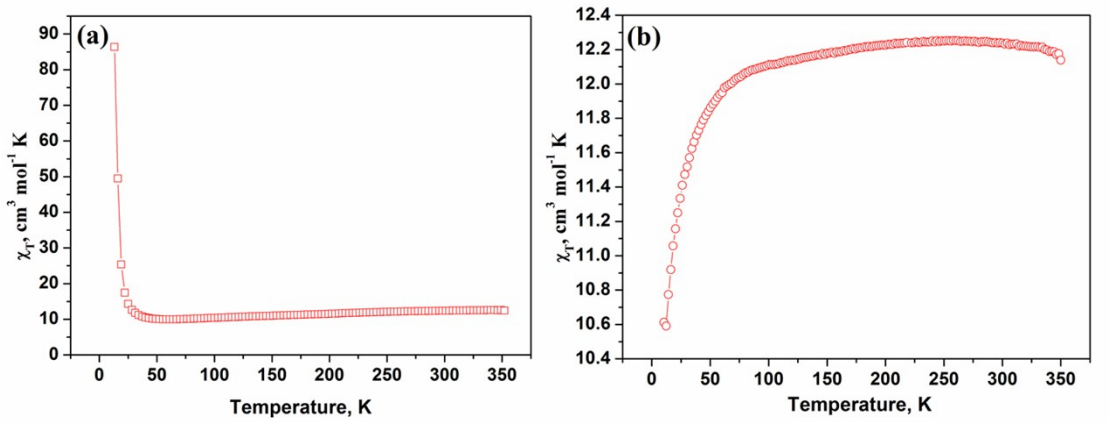

Fig. S9. Magnetization curves of (a) Co-Fe PBA and (b) Fe-Co PBA. $x_T=[Ng^2(s+1)s]/8$ is applied to calculate x based on the assumption that cobalt when bound to nitrogen is high-spin, while cobalt when bound to carbon is low-spin and the calculation results are consistent with the measured magnetization curves.

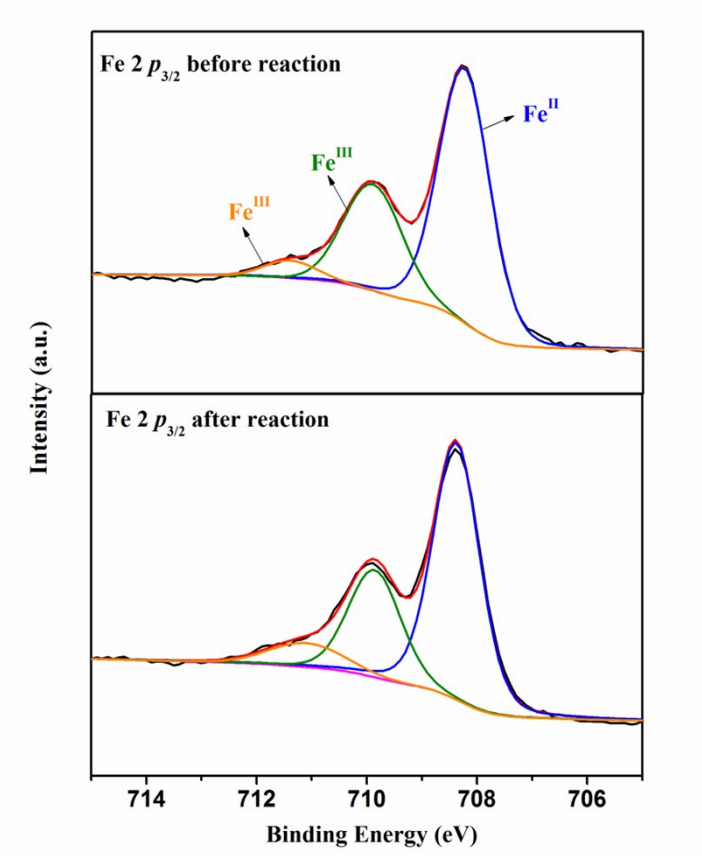

Fig. S10. High resolution XPS results of Fe $2p_{3/2}$ in Co-Fe PBA before and after catalytic reaction.

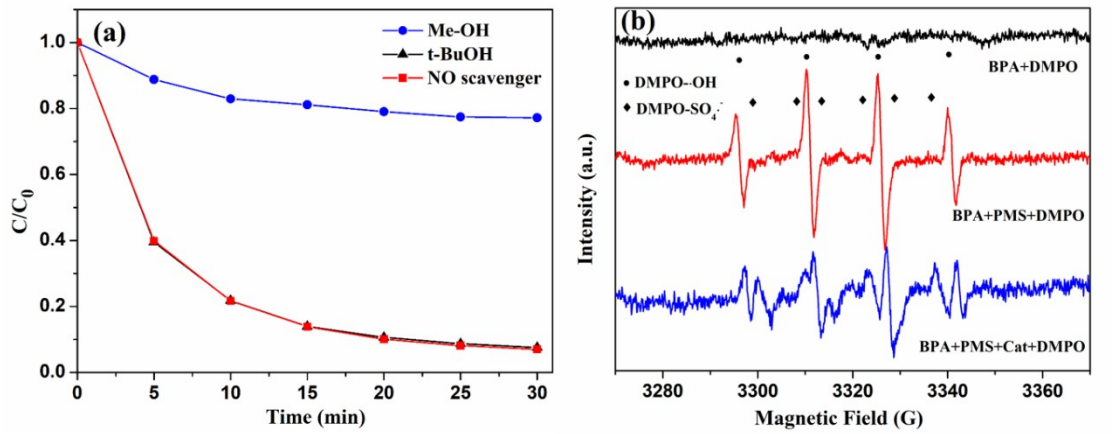

Fig. S11. (a) The quenching experiments of BPA degradation with Co-Fe PBA in the presence of methanol and tert-butyl alcohol; (b) ESR spectra of various simulated systems. Reaction conditions: [BPA] = 20 mg L^{-1}, [PMS] = 0.1 g L^{-1}, catalyst = 0.1 g L^{-1} , T = 308 K, initial solution pH = 6.0.

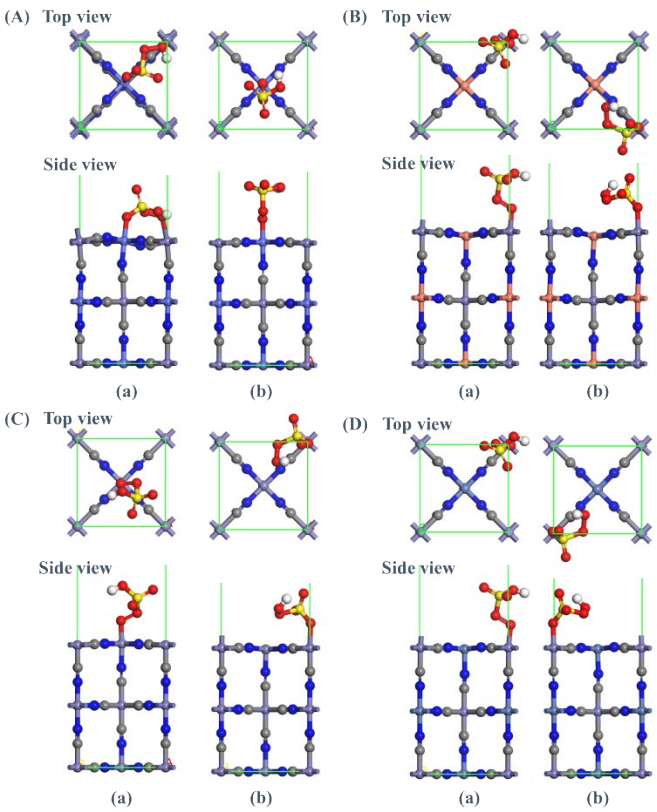

Fig. S12. The most stable structure [panel (a)] and the sub-stable structure [panel (b)] of PMS adsorbed on the Co-Fe PBAs (A), the Cu-Fe PBAs (B), the Fe-Fe PBAs (C) and Ni-Fe PBAs along (200) surface under spin conditions. The gray, blue, red, yellow, white, purple, nattier blue, salmon pink and dusty blue spheres in this and following figures are C, N, O, S, H, Fe, Co, Cu and Ni atoms, respectively.

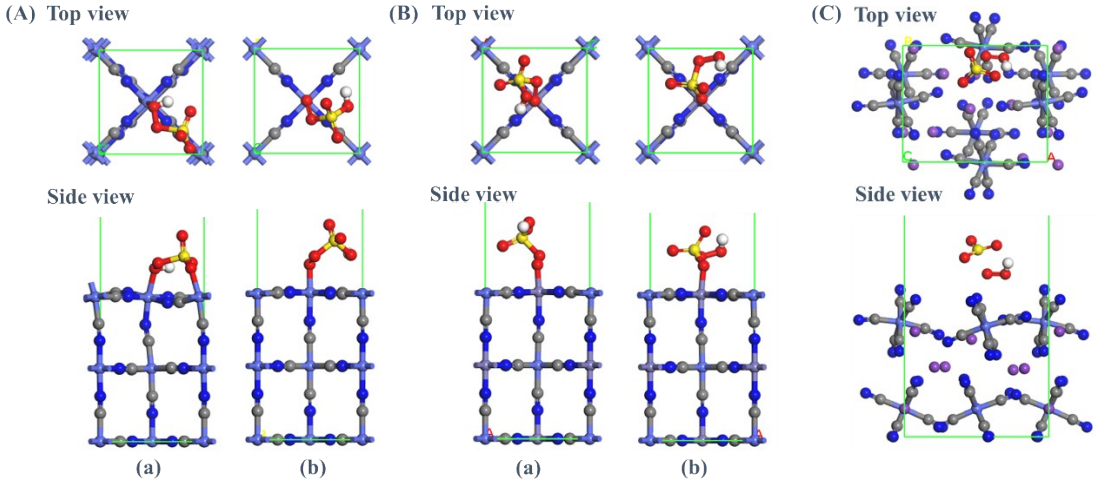

Fig. S13. The most stable structure [panel (a)] and the sub-stable structure [panel (b)] of PMS adsorbed on the Co-Co PBAs (A), the Fe-Co PBAs (B) and the K-Co PBAs (C) along (200) surface under spin conditions. The modena sphere in this figures is K atom.

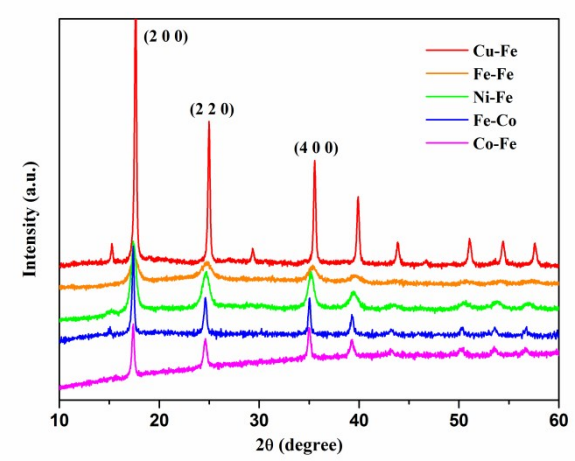

Fig. S14. XRD patterns of M-Fe PBAs (M = Cu, Fe, Ni, Co), and Fe-Co PBA

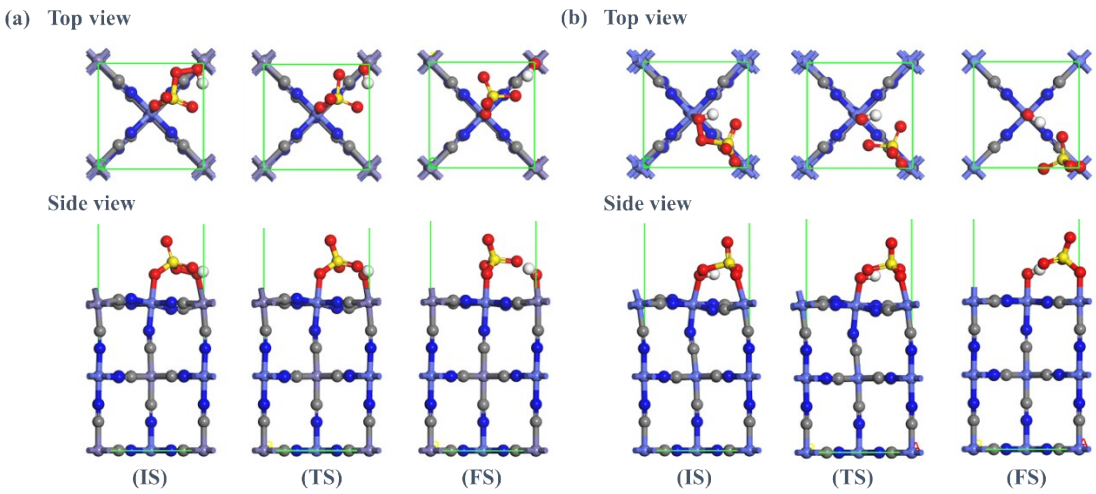

Fig. S15. The detailed structures of PMS on Co-Fe PBA (a) and Co-Co PBA (b) during the activation reaction, where IS, TS and FS represent initial structure, transition structure and final structure of the reaction, respectively.

Table S4. The DFT calculation results for PMS adsorption on different PBAs along (200) surface under spin conditions. – denotes structure rearrangement and such parameter is unavailable. lO–O: the O–O bond length of SO4–OH; Q: the electron transfer from PBAs to PMS; Eads: the adsorption energies of PMS.

PBA type			$l_{O\text{-}O}$ (Å)	Q (e)	E_{ads} (eV)
Non-Co PBAs	Cu-Fe	most stable	-	-	-1.400
		sub-stable	1.419	-0.237	-1.206
	Fe-Fe	most stable	-	-	-1.560
		sub-stable	1.426	-0.324	-1.447
	Ni-Fe	most stable	-	-	-1.474
		sub-stable	1.422	-0.276	-1.335
Co-PBAs	Co-Fe	most stable	1.466	-0.264	-1.704
		sub-stable	-	-	-1.387
	Co-Co	most stable	1.456	-0.270	-1.887
		sub-stable	-	-	-1.568
	Fe-Co	most stable	-	-	-1.735
		sub-stable	1.435	-0.331	-1.636
Precursor	K-Co	most stable	-	-	-0.364

Notes and references

1 X. N. Li, J. Wang, A. I. Rykov, V. K. Sharma, H. Z. Wei, C. Z. Jin, X. Liu, M. R. Li, S. H. Yu, C. L. Sun and D. D. Dionysiou, *Catal. Sci. Technol*, 2015, **5**, 504.

2 B. Delley, *J. Phys. Chem*, 2000, **113**, 7756-7764.

3 G. Henkelman and H. Jónsson, *J. Phys. Chem*, 2000, **113**, 9978-9985.

4 X. Duan, Z. Ao, H. Zhang, M. Saunders, H. Sun, Z. Shao and S. Wang, *Appl. Catal. B*, 2018, **222**, 176-181.

5 Z. M. Ao, F. M. Peeters, *J. Phys. Chem. C*, 2010, **114**, 4503–14509.

6. X. Li, J. Liu, A. I. Rykov, H. Han, C. Jin, X. Liu and J. Wang, *Applied Catalysis B: Environmental*, 2015, 179, 196-205.

7. H. Wang, C. Wang, J. Qi, Y. Yan, M. Zhang, X. Yan, X. Sun, L. Wang and J. Li, *Nanomaterials (Basel)*, 2019, 9.

8. Y. Pi, L. Ma, P. Zhao, Y. Cao, H. Gao, C. Wang, Q. Li, S. Dong and J. Sun, *J Colloid Interface Sci*, 2018, 526, 18-27.

9. Q. Gao, J. Chen, Q. Li, J. Zhang, Z. Zhai, S. Zhang, R. Yu and X. Xing, *Inorganic Chemistry Frontiers*, 2018, 5, 438-445.